Monthly Notices
of the
ROYAL ASTRONOMICAL SOCIETY

MNRAS **466,** 4083–4093 (2017)
Advance Access publication 2017 January 9

doi:10.1093/mnras/stx012

Radio monitoring of protoplanetary discs

C. Ubach,[1,2★] S. T. Maddison,[2] C. M. Wright,[3] D. J. Wilner,[4] D. J. P. Lommen[5] and B. Koribalski[6]

[1]*National Radio Astronomy Observatory, 520 Edgemont Road, Charlottesville, VA 22903-4608, USA*
[2]*Centre for Astrophysics and Supercomputing, Swinburne University of Technology, H30, PO Box 218, Hawthorn, VIC 3122, Australia*
[3]*School of Physical, Environmental and Mathematical Sciences, UNSW@ADFA, Canberra, ACT 2600, Australia*
[4]*Harvard–Smithsonian Center for Astrophysics, 60 Garden Street, Cambridge, MA 02138, USA*
[5]*Hwa Chong Institution, 661 Bukit Timah Road, Singapore 269734*
[6]*CSIRO Astronomy and Space Science, Australia Telescope National Facility (ATNF), PO Box 76, Epping NSW 1710, Australia*

Accepted 2017 January 4. Received 2016 December 31; in original form 2015 September 22

ABSTRACT

Protoplanetary disc systems observed at radio wavelengths often show excess emission above that expected from a simple extrapolation of thermal dust emission observed at short millimetre wavelengths. Monitoring the emission at radio wavelengths can be used to help disentangle the physical mechanisms responsible for this excess, including free–free emission from a wind or jet, and chromospheric emission associated with stellar activity. We present new results from a radio monitoring survey conducted with Australia Telescope Compact Array over the course of several years with observation intervals spanning days, months and years, where the flux variability of 11 T Tauri stars in the Chamaeleon and Lupus star-forming regions was measured at 7 and 15 mm, and 3 and 6 cm. Results show that most sources are variable to some degree at 7 mm, indicating the presence of emission mechanisms other than thermal dust in some sources. Additionally, evidence of grain growth to centimetre-sized pebbles was found for some sources that also have signs of variable flux at 7 mm. We conclude that multiple processes contributing to the emission are common in T Tauri stars at 7 mm and beyond, and that a detection at a single epoch at radio wavelengths should not be used to determine all processes contributing to the emission.

Key words: radiation mechanisms: thermal – protoplanetary discs – radio continuum: planetary systems.

1 INTRODUCTION

Signatures of centimetre-sized pebbles have been detected in protoplanetary discs by extending the relationship between the dust opacity index, β, and the 1 to 3 mm spectral slope, α, to longer centimetre wavelengths (e.g. Testi et al. 2003; Wilner et al. 2005; Rodmann et al. 2006; Lommen et al. 2009). The results from this relationship ($\beta \sim \alpha - 2$) can indicate grain growth up to 3λ (where λ is the observed wavelength) when $\beta < 1$, and limited to no grain growth (interstellar-medium-sized grains) for $\beta > 1$, as long as the grain size $\ll\lambda$ (Draine 2006).

This approach assumes that the long wavelength emission follows the 1–3 mm emission, which is dominated by thermal dust emission and is constant over time, which is not always the case at longer wavelengths (e.g. Lommen et al. 2010; Ubach et al. 2012).

A dozen protoplanetary discs show a 'break' in the spectral slope near 7 mm, with a shallower spectral slope at longer wavelengths (Rodmann et al. 2006; Lommen et al. 2009, 2010; Ubach et al. 2012). This 'break' has been attributed to emission mechanisms related to ionized plasma, adding to the emission from thermal dust in these discs. This excess emission at long millimetre wavelengths could be caused by either thermal free–free emission from an ionized wind or by non-thermal processes such as chromospheric emission from the young star, or a combination of both. At 7 mm, both thermal dust emission and thermal free–free emission from an ionized wind have been detected in young stellar objects (YSOs; e.g. Rodmann et al. 2006; Lommen et al. 2009), while variable emission at 3 and 6 cm has been used to demonstrate a combination of all three emission mechanisms (e.g. Lommen et al. 2009).

Temporal monitoring of the disc emission has been used to disentangle these three emission mechanisms (Lommen et al. 2009; Ubach et al. 2012). Flux originating from thermal dust emission is generally assumed to be constant over time, whereas the flux from thermal free–free and non-thermal emission may be temporally variable. Thermal free–free emission can vary by a factor of ∼20–40 per cent over a time-scale measured in years (Skinner & Brown 1994; González & Cantó 2002; Smith et al. 2003; Lommen

★ E-mail: cubach@nrao.edu

Table 1. List of the 11 sources observed with ATCA in this survey.

Source	RA (J2000)	Dec. (J2000)	Cloud	Distances (pc)	$T_{\rm eff}$ (K)	Wavelengths (mm)
			Chamaeleon			
CR Cha	10 59 06.9	−77 01 39.7	Cha I	160	4900	7
CS Cha$^{\Phi}$	11 02 24.9	−77 33 35.9	Cha I	160	4205	7, 15
DI Cha$^{\Phi}$	11 07 21.6	−77 38 12.0	Cha I	160	5860	7
T Cha	11 57 13.6	−79 21 31.7	Isolated	100	5600	7, 30, 60
Glass I$^{\Phi}$	11 08 15.1	−77 33 59.0	Cha I	160	5630	7
SZ Cha	10 58 16.7	−77 17 17.1	Cha I	160	5250	7, 15
Sz 32	11 09 53.4	−76 34 25.5	Cha I	160	4350	7, 30, 60
WW Cha	11 10 00.1	−76 34 57.9	Cha I	160	4350	7, 30, 60
			Lupus			
Sz 111	16 08 54.7	−39 37 43.1	Lupus 4	200	3573	7, 15
MY Lup	16 00 44.6	−41 55 29.6	Lupus 3	165	5248	7, 15
GQ Lup	15 49 12.1	−35 39 03.9	Lupus 1	156	4300	7, 15

Distances and effective temperatures taken from: (1) Whittet et al. (1997), (2) van den Ancker, de Winter & Tjin A Djie (1998), (3) Luhman (2004), (4) Hughes et al. (1994), (5) Comerón (2008), (6) Neuhäuser et al. (2008), (7) Donati et al. (2012).
$^{\Phi}$Binary separations of $\leq$1, 4.6 and 2.5 arcsec for CS Cha, DI Cha and Glass I, respectively (Guenther et al. 2007; Ghez et al. 1997; Feigelson & Kriss 1989).

et al. 2009), while non-thermal emission mechanisms may vary by a factor of 2 or more on time-scales of hours to days (Kuijpers & van der Hulst 1985; Phillips, Lonsdale & Feigelson 1991, 1993; Skinner & Brown 1994; Chiang, Phillips & Lonsdale 1996; Smith et al. 2003).

Here, we present continuum flux monitoring of T Tauri stars at 7 and 15 mm, and 3 and 6 cm over time-scales of days, months and years. We analyse the data to determine the various contributing emission mechanisms present in the discs. We further determine whether it is common for protoplanetary discs to show evidence both of grain growth up to centimetre-sized pebbles and of multiple emission mechanisms.

2 OBSERVATIONS AND DATA REDUCTION

This survey targeted 11 T Tauri stars in the Chamaeleon and Lupus star-forming regions – see Table 1. The sources were selected to overlap with the Lommen et al. (2009, 2010) and Ubach et al. (2012) samples, maximizing the number of sources and increasing the monitoring baseline to years – see Tables A1 and A2.

Continuum observations were conducted with Australia Telescope Compact Array (ATCA) during the winter 2012 season. Three compact hybrid array configurations were used, providing synthesized beams between 5 and 15 arcsec at 7 mm, corresponding to $\sim$800 − 2400 au assuming a distance of 160 pc to the sources. The two CABB[1] intermediate frequency bands were divided into 2048 channels of 1 MHz width.

All targets were observed with frequency pairs centred at 43 + 45 GHz (7 mm band), five targets[2] at 17 + 19 GHz (15 mm band) and three targets at 5.5 + 9.9 GHz (6 and 3 cm bands, respectively). The millimetre frequency bands setup provided a 4 GHz wide band with an expected rms of 0.1 and 0.03 mJy for 30 min on source for the 7 and 15 mm bands, respectively. The 3 and 6 cm bands were 2 GHz wide with an expected rms of 0.027 and 0.034 mJy for 30 min on source, respectively. In total, this survey covered frequencies ranging from 4.5 to 46 GHz.

QSO B1057−79 and QSO B1600−44 were used as gain calibrators for Chamaeleon and Lupus, respectively. For all the observations the absolute flux calibration was performed using PKS 1934−638. Weather conditions were good throughout the observations. Due to poor u–v coverage at the longer baselines when using the compact hybrid arrays, and given that fluxes rather than images were the required data products, antenna 6 was not included in the data processing and analysis.

The data calibration followed the standard CABB procedure described in the ATCA user guide[3] for all wavelengths using the software package MIRIAD version 1.5 (Sault, Teuben & Wright 1995). In order to determine the source fluxes, we used a point source fit. To ensure that this was appropriate, we checked the visibility amplitudes were constant over u–v distance for all 11 sources at each epoch.

For this analysis, the data from each day at each frequency were calibrated separately and then the frequency pairs were combined. The flux (from the point source fit) and rms values for all observations were then extracted from the visibilities using UVFIT and UVRMS.

3 RESULTS AND DISCUSSION

A summary of the continuum fluxes for the combined frequency pairs are presented in Table 2, complemented with fluxes obtained from literature. The detection rates for the sources observed in this study are as follows: 9/11 sources were detected at 7 mm, 3/5 at 15 mm[4] and 0/3 sources at both 3 and 6 cm. A 3σ upper limit is provided for non-detections.

We present in Fig. 1 both the spectrum or radio flux as a function of wavelength (left-hand panels), and the 7 mm flux versus time (right-hand panels) for the 11 sources in our survey. Detections are denoted by a star symbol and upper limits by an arrow. Error bars include the uncertainty in the flux fit, as well as the primary flux

[1] Compact Array Broad-band Backend (Wilson et al. 2011).
[2] Only two of the sources have previous 15 mm observations.

[3] http://www.narrabri.atnf.csiro.au/observing/users_guide/html/atug.html. For specific data reduction procedure see Ubach (2014).
[4] See Table B1 for results of sources observed at 15 mm with no previously reported 15 mm fluxes.

Table 2. Summary of the temporal monitoring results at 7 and 15 mm, and 3 and 6 cm for our sample of 11 T Tauri stars. (1) Source name. (2) Julian date of the observation. (3) Time from previous observation in days. (4) Combined frequency. (5) Point flux (3σ upper limit for non-detections). (6) rms. (7) Reference. See Table B1 for new 15 mm observations of sources with no previously reported 15 mm fluxes.

(1) Source	(2) Julian date	(3) Time from previous observation (d)	(4) Frequency (GHz)	(5) Flux (mJy)	(6) rms (mJy beam^{-1})	(7) Reference
CR Cha	245 4980	–	44	1.7 ± 0.1	0.1	Ubach et al. (2012)
	245 6143	1163	44	1.3 ± 0.2	0.1	This work
CS Cha	245 4583	–	44	1.00 ± 0.28	0.129	Lommen et al. (2009)
	245 4677	94	44	<0.71	0.238	Lommen et al. (2009)
	245 4678	1	44	1.38 ± 0.26	0.218	Lommen et al. (2009)
	245 4980	302	44	1.5 ± 0.1	0.1	Ubach et al. (2012)
	245 6143	1163	44	1.5 ± 0.2	0.1	This work
	245 6223	81	44	0.6 ± 0.1	0.3	This work
	245 5753	–	18	<0.3	0.1	Ubach et al. (2012)
	245 6131	378	18	0.20 ± 0.02	0.03	This work
DI Cha	245 4980	–	44	0.9 ± 0.1	0.1	Ubach et al. (2012)
	245 6143	1163	44	<0.2	0.1	This work
T Cha	245 4980	–	44	3.0 ± 0.1	0.1	Ubach et al. (2012)
	245 6143	1163	44	4.1 ± 0.2	0.1	This work
	245 5761	–	9.9	<0.3	0.1	Ubach et al. (2012)
	245 6123	363	9.9	<0.15	0.05	This work
	245 5761	–	5.5	0.3 ± 0.1	0.1	Ubach et al. (2012)
	245 6123	363	5.5	<0.2	0.08	This work
Glass I	245 4980	–	44	0.6 ± 0.2	0.1	Ubach et al. (2012)
	245 6143	1163	44	<0.3	0.1	This work
SZ Cha	245 4980	–	44	0.7 ± 0.1	0.1	Ubach et al. (2012)
	245 6143	1163	44	0.6 ± 0.1	0.1	This work
	245 6223	81	44	<0.3	0.1	This work
Sz 32	245 4558	–	44	0.8 ± 0.1	0.2	Lommen et al. (2009)
	245 4980	422	44	1.2 ± 0.1	0.2	Ubach et al. (2012)
	245 6143	1163	44	0.5 ± 0.2	0.1	This work
	245 5761	–	9.9	<0.3	0.1	Ubach et al. (2012)
	245 6123	363	9.9	<0.15	0.05	This work
	245 5761	–	5.5	<0.3	0.1	Ubach et al. (2012)
	245 6123	363	5.5	<0.1	0.04	This work
WW Cha	245 4980	–	44	9.1 ± 0.35	0.2	Ubach et al. (2012)
	245 6143	1163	44	3.9 ± 0.2	0.1	This work
	245 5761	–	9.9	<0.3	0.1	Ubach et al. (2012)
	245 6123	363	9.9	<0.15	0.05	This work
	245 5761	–	5.5	<0.45	0.1	Ubach et al. (2012)
	245 6123	363	5.5	<0.12	0.04	This work
Sz 111	245 4680	–	44	<0.6	0.2	Lommen et al. (2010)
	245 4980	300	44	0.5 ± 0.1	0.1	Ubach et al. (2012)
	245 6143	1163	44	0.6 ± 0.2	0.1	This work
	245 6223	81	44	0.4 ± 0.1	0.03	This work
MY Lup	245 4680	–	45	1.3	0.1	Lommen et al. (2010)
	245 4980	300	44	1.1 ± 0.1	0.1	Ubach et al. (2012)
	245 6143	1163	44	1.0 ± 0.2	0.1	This work
	245 6223	81	44	1.2 ± 0.2	0.03	This work
GQ Lup	245 5430	–	44	0.6 ± 0.1	0.04	Ubach et al. (2012)
	245 5753	323	44	0.6 ± 0.3	0.07	Ubach et al. (2012)
	245 6144	391	44	1.2 ± 0.1	0.05	This work
	245 6223	79	44	0.5 ± 0.1	0.04	This work
	245 5751	–	18	0.07 ± 0.03	0.01	Ubach (2014)
	245 5761	10	18	0.08 ± 0.04	0.02	Ubach (2014)
	245 6223	462	18	<0.09	0.03	This work

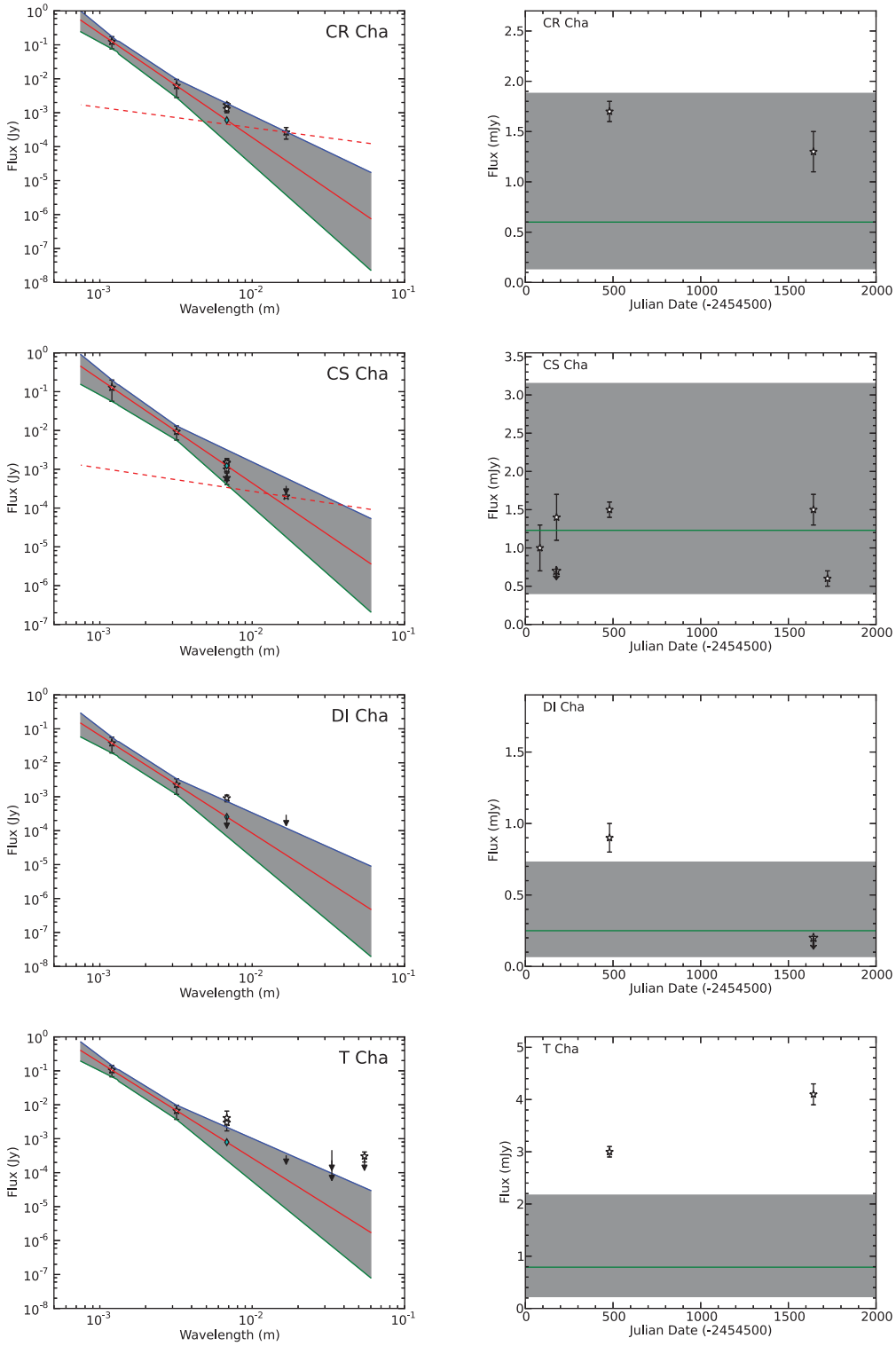

Figure 1. Radio spectrum (left-hand panels) and temporal flux monitoring (right-hand panels) for each source in the survey. Detections are denoted by a star and upper limits by an arrow. Error bars include the flux fit uncertainty and primary flux calibration uncertainties. The red solid line in the spectrum (left-hand panels) represents the 1–3 mm spectral slope α, the red dashed line the expected $\alpha_{\rm ff} = -0.6$ and the grey shaded area represents the region of uncertainly in the estimated thermal dust emission from standard error propagation in the spectral slope calculation. The green diamond (left-hand panels) and green line (right-hand panels) correspond to the estimated thermal dust emission at 7 mm. Continued on the next page.

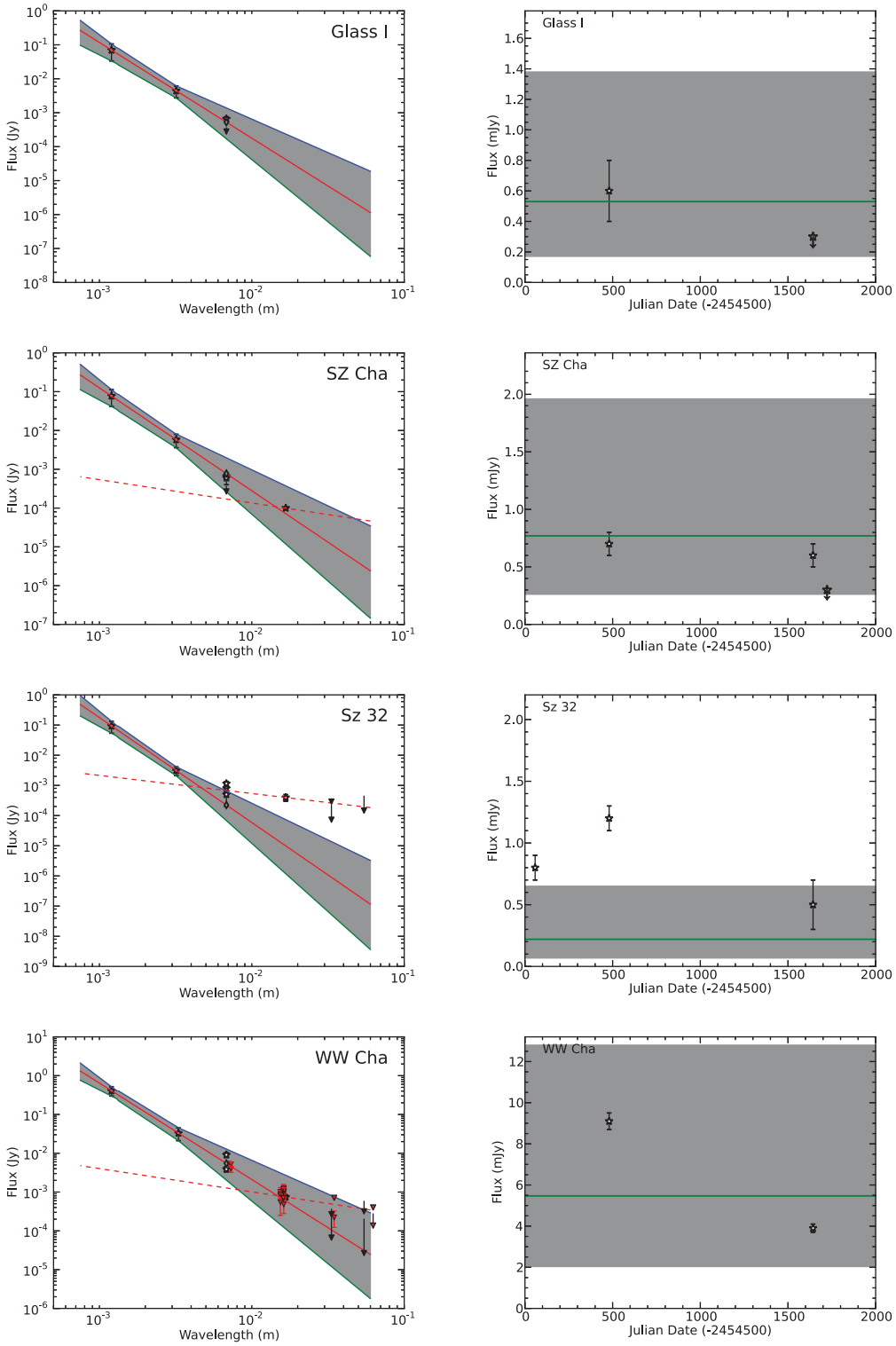

Figure 1 – *Continued.*

calibration uncertainties of 20 per cent for 1.2 mm, 30 per cent for 3 mm, and 10 per cent for 7 mm, 15 mm, 3 cm and 6 cm. In the spectrum plots, the red solid line represents the estimated emission due to thermal dust, which was fit using the least-squares method between the 1 and 3 mm fluxes and extrapolating this spectral slope, α, to longer wavelengths. Fluxes at 1 and 3 mm were taken from Ubach et al. (2012) and references therein. The estimated 7 mm thermal dust component, $F_{7\mathrm{mm}}$(therm), is denoted by a green diamond. The grey shaded area represents the region of uncertainty in the spectral slope using standard quadratic error propagation. If we take a 'slice' through the radio spectrum at 7 mm, and plot each observed 44 GHz flux against time (as presented in Table 2),

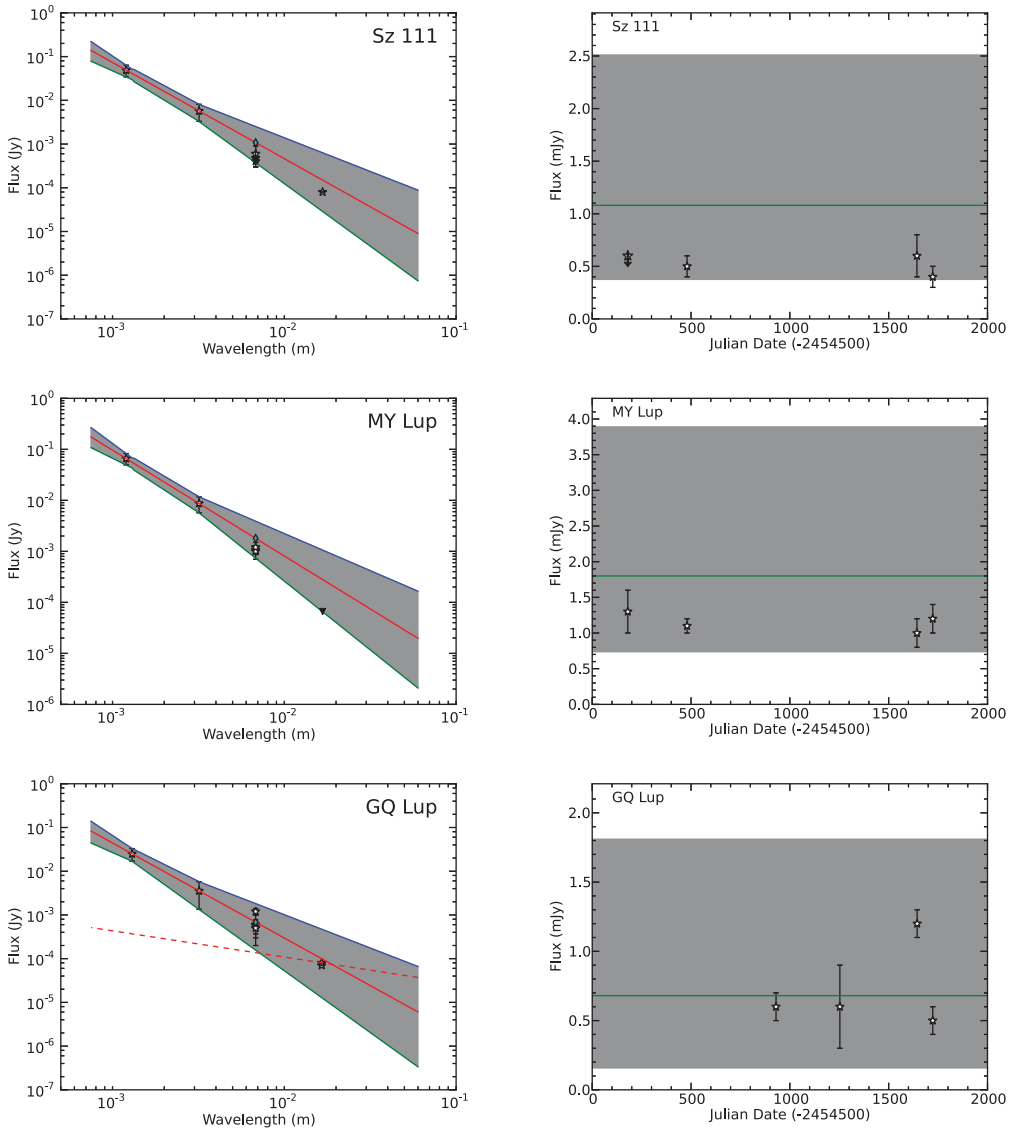

Figure 1 – *Continued.*

this gives us the temporal monitoring plots on the right. Here the grey region is the same as in the spectrum plot, and represents the uncertainty of the extrapolation of the 7 mm thermal flux estimate, $F_{7\mathrm{mm}}$(therm), which is now represented by a green line. We will use both of these plots to help understand the emission processes in each system.

3.1 Temporal monitoring

The aim of our temporal monitoring campaign is to try and disentangle the different physical processes contributing to the radio emission in this sample of T Tauri stars. While a number of millimetre and centimetre surveys of YSOs have been conducted (e.g. Henning et al. 1993; Andrews & Williams 2007), few monitoring surveys have been carried out due to their intense resources requirement. Given that YSOs are inherently variable (e.g. Herbst et al. 1994), flux monitoring on time-scales of a day, weeks and years are required to understand the contributing processes to their emission. Here, we compare fluxes obtained from a few days apart to hundreds of days apart, as presented in Table 2.

From our previous observations (Ubach et al. 2012), our sample could be divided into two distinct groups: (i) those with a constant spectral slope from 1 to 7 mm (CS Cha, Glass I, SZ Cha, WW Cha, MY Lup, Sz 111 and GQ Lup) and (ii) those with a 'break' in the millimetre spectral slope at 7 mm (CR Cha, DI Cha, T Cha and Sz 32). This 'break' is an indication that other forms of emission at 7 mm are present in addition to thermal dust emission. In Ubach et al. (2012), a least-squares fit was used to determine the spectral slope between 1 and 3 mm, α, and extrapolated to 7 mm to estimate the thermal dust component $F_{7\mathrm{mm}}$(therm). Table 3 presents the estimated thermal dust emission at 7 mm, the maximum observed 7 mm flux, $F_{7\mathrm{mm}}$(max), and the fractional 7 mm excess, given by $[F_{7\mathrm{mm}}(\mathrm{max}) - F_{7\mathrm{mm}}(\mathrm{therm})]/F_{7\mathrm{mm}}(\mathrm{therm})$, for this sample of 11 protoplanetary discs.

Using a combination of the spectrum and the temporal monitoring plots in Fig. 1, along with the data in Table 3, we can start to understand the degree and potential source of variability in each

Table 3. Summary of 7 mm analysis of the spectral slope, estimated 7 mm thermal dust emission, maximum 7 mm emission observed and the fractional 7 mm excess above thermal. The α values are from Ubach et al. (2012), except for WW Cha that was obtained from Lommen et al. (2009). The estimated thermal dust is obtained by extrapolating α to 44 GHz. The fractional 7 mm excess above thermal is the estimated 7 mm excess, $[F_{7mm}(\max) - F_{7mm}(\text{therm})]$, divided by the estimated thermal dust, $F_{7mm}(\text{therm})$.

Source	α	F_{7mm}(therm) (mJy)	F_{7mm}(max) (mJy)	Fractional 7 mm excess
CR Cha	3.4	0.6	1.7	1.8
CS Cha	2.9	1.2	1.5	0.3
DI Cha	3.2	0.3	0.9	2.0
T Cha	3.1	0.8	4.1	4.1
Glass I	3.1	0.5	0.6	0.2
SZ Cha	2.9	0.8	0.7	−0.1
Sz 32	3.8	0.2	1.2	5.0
WW Cha	2.8	5.5	9.1	0.7
Sz 111	2.5	1.1	0.6	−0.5
MY Lup	2.3	1.8	1.2	−0.3
GQ Lup	2.2	0.7	1.2	0.7

system.[5] If we start with the (crude) fractional 7 mm excess, we can place the 11 sources into three groups: those with high to extreme fractional excesses above 1.5; those with a moderate fractional excess between 0.5 and 1.0; and those with a small fractional excess less than 0.5.

Of the high to extreme 7 mm fractional excess sources, we can see that CR Cha and DI Cha have excesses of order 2 above expected thermal dust, while T Cha and Sz 32 have much larger excesses of order 4–5. Looking at the radio spectrum of the two most extreme sources, we can clearly see a break in the spectral slope at 7 mm, excess emission and flux variability in T Cha and Sz 32. Their 7 mm temporal monitoring plots show fluxes well in excess of that estimated for thermal dust, i.e. the observed fluxes are outside of the grey regions of the plots. Over the 3 yr period of the observations, the 7 mm fluxes of T Cha and Sz 32 varied by a factor of ∼0.4 and 1.4, respectively. The 3 and 6 cm flux monitoring of both sources also suggests variably over the course of a year by 30–50 per cent, and detailed analysis of the 15 mm and 3 + 6 cm intra-epoch fluxes by Ubach et al. (2012) show variability of a factor of 2 on the time-scale of tens of minutes. There is also a break in the spectral slope at 7 mm seen in CR Cha and DI Cha, and over the 3 yr period of 7 mm observations, both show variably of a factor of 0.3 and 3, respectively. They have only a single observation at 15 mm and intra-epoch analysis by Ubach et al. (2012) of CS Cha shows 15 mm variability of a factor of 2 on time-scales of tens of minutes. For all four sources it seems likely that a mix of thermal dust, thermal free–free emission and non-thermal processes contribute to the radio emission.

The sources with moderate fractional excess include WW Cha and GQ Lup. None of these sources have a break in their spectral slope at 7 mm, and their 7 mm fluxes all lie within the region of uncertainty of the extrapolated 7 mm thermal dust emission. Three of the four 7 mm fluxes recorded for GQ Lup over a 2.2 yr period are consistent, though there is variability of a factor of 2.4 in just

[5] Note that the fractional 7 mm excess presented in Table 3 does not take into consideration the errors in the estimated 7 mm thermal dust emission, and so can only be considered a very crude measure of any emission excess above thermal dust.

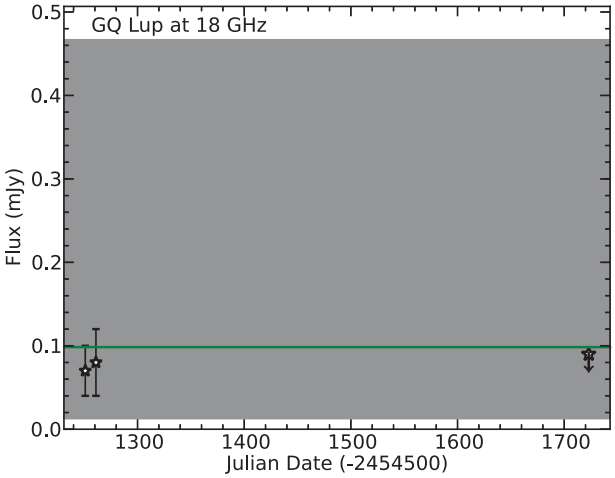

Figure 2. The 15 mm continuum fluxes for GQ Lup plotted from the first recorded epoch. The error bars represented the flux uncertainties. No flux variability was observed over a year time-scale, suggesting the emission detected is primarily from thermal dust. The green diamond symbol/line correspond to the thermal dust emission component of the fluxes at 15 mm, error bars are the uncertainties for the estimated value.

under three months. GQ Lup was also observed at 15 mm over a period of almost 1.3 yr, and all three fluxes are consistent within the flux fit errors – see Fig. 2. While not exactly simultaneous, the two 7 mm and 15 mm observations that were made about 470 d apart give consistent (non-varying) fluxes in both bands.

There have been many observations of WW Cha – see Table C1 for a summary. In Table 2, we present just the 44, 18, 9.9 and 5.5 GHz observations for the sources in our survey, while as it can be seen in Table C1, WW Cha has been observed at various wavelengths in the 7 mm, 15 mm, and 3 and 6 cm bands. In the spectrum of WW Cha in Fig. 1, we present all the data from Table C1, with the red inverted triangles representing detections and upper limits obtained by Lommen et al. (2009). The 7 mm monitoring data show only the 44 GHz data for consistency. The centimetre-band data clearly show a lot of variability, by factors of 2–4, and the two 7 mm fluxes taken 3.2 yr apart vary by a factor of 2.3. With the radio monitoring data to date, it appears that Sz 111 and GQ Lup are dominated by thermal dust emission, though there is variability at 7 mm in GQ Lup. WW Cha likely has a mix of thermal dust, thermal free–free emission and non-thermal processes contributing to the radio emission.

The sources with low fractional excess include CS Cha and Glass I. Once again, none show a break in their spectral slope at 7 mm, and their 7 mm fluxes all lie within the region of uncertainty of the extrapolated 7 mm thermal dust estimate. Glass I vary by a factor of 2.3 and 2 over 3.2 yr. CS Cha varies by about a factor of 3 over 3 months. This magnitude of variability for Glass I and CS Cha suggests that the non-thermal emission as well as thermal dust contribute to the overall emission.

Finally, we find that just three sources in our sample, SZ Cha, Sz 111 and MY Lup, have no observed variability at 7 mm over a time-scale of hundreds of days, suggesting that the detected continuum flux emission is due to thermal dust emission, whereas all other sources exhibit flux variability on the time-scale of months to years of at least 30 per cent and up to a factor of 3 at 7 mm is observed, which provides evidence of the presence of excess emission from mechanisms other than thermal dust emission. However, the 7 mm fluxes for these three sources are also lower than expected from spectral fit. This perhaps is indicative that the calculated α is too

shallow. This appears to be supported by the lower 15 mm fluxes in Sz 111 and MY Lup. This survey highlights the significance of flux monitoring over multiple time-scales, for one flux detection will not always be a good indication of a pure thermal dust emission source at 7 mm and beyond.

3.2 Grain growth

For this sample of 11 protoplanetary discs, the two sources with no detected flux variability at 7 mm, MY Lup and Sz 111, also have $\alpha < 3$. The four sources with high to extreme 7 mm fractional excess all have $\alpha > 3$, while all sources with moderate to low fractional excess – with the exception of Glass I – have $\alpha < 3$. Applying the simplified Draine (2006) relationship of $\beta \sim \alpha - 2$, our results suggest that the majority of the sources have $\beta < 1$, indicative of grain growth up to cm sizes, and the four most active sources with clear signs of excess emission above thermal dust have $\beta > 1$, suggesting little grain growth. These results show that both variability and evidence for grain growth can be present for the same protoplanetary disc, but that grain growth appears inhibited in the most active sources, at least for this small sample.

3.3 Excess emission at millimetre wavelengths

We have thus far determined that the presence of emission mechanisms other than thermal dust emission at 7 mm is common in protoplanetary discs, and that signatures of grain growth can be found in sources with and without 7 mm flux variability. The 7 mm flux variability of ∼30 per cent over a period of hundreds of days is consistent with the characteristics of thermal free–free emission. The presence of flux variability has also been detected at other wavelengths, such as in the X-ray, optical and in the near-infrared (NIR).

All the sources in our sample (with the exception of MY Lup and Sz 111) have been detected in the X-ray with a $\log(L_X/L_{bol})$ between −3 and −4, classifying these stars as X-ray active (e.g. Feigelson & Lawson 2004; Stelzer, Micela & Neuhäuser 2004). A few sources in our sample have been studied more closely in the literature. Using the *XMM–Newton* observations of CR Cha, Robrade & Schmitt (2006) detected a small flare and flux variability consistent with coronal activity and the presence of accretion. CS Cha, T Cha and GQ Lup were included in Güdel et al. (2010) analyses of *Spitzer* [Ne II] line and *XMM–Newton* archive data, where they classified CS Cha as a jet-driving object with a transitional disc, T Cha as a transitional disc and GQ Lup as an optically thick disc without a known jet. Similarly, X-ray flares have also been detected for Sz 32 and WW Cha (Feigelson & Lawson 2004). It is interesting to note that sources with flux variability at millimetre wavelengths are also variable in the X-ray; specifically the sources with high amplitude variability in the radio (CS Cha, GQ Lup, Sz 32, WW Cha) are also very active in the X-ray. This suggests that the cause of the variability could be the same at both wavelengths. Simultaneous observations at both wavelengths would be needed to confirm this relationship.

Flux variability of up to 20 per cent is commonly found in YSOs in the optical and NIR wavebands (Scholz 2012; Rodgers-Lee et al. 2014). This variability can be caused by hotspots created by an accretion shock, variable circumstellar extinction or a combination of these processes (Scholz 2012). Although variability above 20 per cent in the optical and NIR is rare, it has been documented. Additional optical images in the *R* and *I* bands and NIR images in the *J* and *K* bands have provided evidence that Sz 32 is variable at these wavelengths by more than the expected 20 per cent (Rodgers-Lee et al. 2014). The cause of the additional flux variability is still under investigation.

4 CONCLUSIONS

We present a radio flux monitoring survey of 11 T Tauri stars in the Chamaeleon and Lupus southern star-forming regions over time-scales of hundreds of days. We found that the 7 mm flux varies by at least 30 per cent and up to a factor of 3 for most sources, indicating that processes other than just thermal dust are contributing to the emission. Flux monitoring of CS Cha and GQ Lup at 15 mm over the course of a year found consistent fluxes, suggesting no variability over these time-scales for these observations. Monitoring of T Cha, Sz 32 and WW Cha at 3 and 6 cm also suggests excess emission above thermal dust. From our analysis of the radio spectrum and flux monitoring, only two sources show no variability and seem to be dominated by thermal dust emission: Sz 111 and MY Lup.

Additionally, we looked at the flux variability in the X-ray, optical and NIR wavelengths, and found further support for the need for multiple epoch and multiwavelength observations to determine the cause of the flux variability.

We found seven sources with $\beta < 1$, indicative of grain growth up to centimetre-sized grains and four sources with a $\beta > 1$, suggesting little to no grain growth. These results, with the exception of Sz 32, are consistent with reported values for spectral slope from 1 to 3 mm. Of the seven sources with signatures of grain growth, only CR Cha and MY Lup have no reported 7 mm flux variability. Thus, these results show that both signatures of grain growth and evidence of other emission mechanism at 7 mm may be present for the same protoplanetary disc.

In the near future, the high resolution and sensitivity of Atacama Large Millimeter/Submillimeter Array will play an important role in answering these questions by significantly reducing the uncertainties in the 1 mm fluxes for the Chamaeleon sources, and thus reducing the uncertainties in the 1–3 mm spectral slope and β values, and providing a better understanding of the signatures of grain growth in these protoplanetary discs.

ACKNOWLEDGEMENTS

We thank Hans Guenther and Scott Wolk for their help with the XMM-Newton Serendipitous Source Catalogue and for helpful discussions. We also thank Leondardo Testi for useful discussions, and the referee for their useful comments and constructive feedback. The Australia Telescope Compact Array is part of the Australia Telescope National Facility, which is funded by the Commonwealth of Australia for operation as a National Facility managed by CSIRO. This research was supported in part by a Swinburne University Postgraduate Research Award and CSIRO OCE Postgraduate Top Up Scholarship. CMW acknowledges support from the Australian Research Council through Discovery Grant DP0345227 and Future Fellowship FT100100495.

REFERENCES

Andrews S. M., Williams J. P., 2007, ApJ, 671, 1800
Chiang E., Phillips R. B., Lonsdale C. J., 1996, AJ, 111, 355
Comerón F., 2008, in Reipurth B. ed., ASP Monograph Publications, Vol. 5, Handbook of Star Forming Regions, Volume II: The Southern Sky. ASP Monograph Publ., San Francisco, CA, p. 295
Donati J.-F. et al., 2012, MNRAS, 425, 2948

Draine B. T., 2006, ApJ, 636, 1114
Feigelson E. D., Kriss G. A., 1989, ApJ, 338, 262
Feigelson E. D., Lawson W. A., 2004, ApJ, 614, 267
Ghez A. M., McCarthy D. W., Patience J. L., Beck T. L., 1997, ApJ, 481, 378
González R. F., Cantó J., 2002, ApJ, 580, 459
Güdel M. et al., 2010, A&A, 519, A113
Guenther E. W., Esposito M., Mundt R., Covino E., Alcalá J. M., Cusano F., Stecklum B., 2007, A&A, 467, 1147
Henning T., Pfau W., Zinnecker H., Prusti T., 1993, A&A, 276, 129
Herbst W., Herbst D. K., Grossman E. J., Weinstein D., 1994, AJ, 108, 1906
Hughes J., Hartigan P., Krautter J., Kelemen J., 1994, AJ, 108, 1071
Kuijpers J., van der Hulst J. M., 1985, A&A, 149, 343
Lommen D., Wright C. M., Maddison S. T., 2007, A&A, 462, 211
Lommen D., Maddison S. T., Wright C. M., van Dishoeck E. F., Wilner D. J., Bourke T. L., 2009, A&A, 495, 869
Lommen D. J. P. et al., 2010, A&A, 515, A77
Luhman K. L., 2004, ApJ, 602, 816
Neuhäuser R., Mugrauer M., Seifahrt A., Schmidt T. O. B., Vogt N., 2008, A&A, 484, 281
Phillips R. B., Lonsdale C. J., Feigelson E. D., 1991, ApJ, 382, 261
Phillips R. B., Lonsdale C. J., Feigelson E. D., 1993, ApJ, 403, L43
Robrade J., Schmitt J. H. M. M., 2006, A&A, 449, 737
Rodgers-Lee D., Scholz A., Natta A., Ray T., 2014, MNRAS, 443, 1587
Rodmann J., Henning T., Chandler C. J., Mundy L. G., Wilner D. J., 2006, A&A, 446, 211
Sault R. J., Teuben P. J., Wright M. C. H., 1995, in Shaw R. A., Payne H. E., Hayes J. J. E., eds, ASP Conf. Ser. Vol. 77, Astronomical Data Analysis Software and Systems IV. Astron. Soc. Pac., San Francisco, p. 433
Scholz A., 2012, MNRAS, 420, 1495
Skinner S. L., Brown A., 1994, AJ, 107, 1461
Smith K., Pestalozzi M., Güdel M., Conway J., Benz A. O., 2003, A&A, 406, 957
Stelzer B., Micela G., Neuhäuser R., 2004, A&A, 423, 1029
Testi L., Natta A., Shepherd D. S., Wilner D. J., 2003, A&A, 403, 323
Ubach C., 2014, PhD thesis, Swinburne Univ. Technology, Melbourne
Ubach C., Maddison S. T., Wright C. M., Wilner D. J., Lommen D. J. P., Koribalski B., 2012, MNRAS, 425, 3137
van den Ancker M. E., de Winter D., Tjin A Djie H. R. E., 1998, A&A, 330, 145
Whittet D. C. B., Prusti T., Franco G. A. P., Gerakines P. A., Kilkenny D., Larson K. A., Wesselius P. R., 1997, A&A, 327, 1194
Wilner D. J., D'Alessio P., Calvet N., Claussen M. J., Hartmann L., 2005, ApJ, 626, L109
Wilson W. E. et al., 2011, MNRAS, 416, 832

APPENDIX A: OBSERVING LOGS

Table A1. ATCA observing log for Lupus sources from this work and literature. (1) Source name. (2) Date of observations. (3) Frequency pair. (4) Flux calibrator. (5) ATCA array configuration. (6) Synthesized beam size. (7) Total integration time used for analysis. (8) rms. (9) Reference.

(1) Source	(2) Date	(3) Frequency pair (GHz)	(4) Flux Calibrator	(5) Antenna(s) Configuration	(6) Beam size arcsec	(7) T_{int} (min)	(8) rms (mJy beam^{-1})	(9) Reference
Sz 111	Aug 8	43 + 45	Uranus	H214	4	–	0.2	Lommen et al. (2010)
	May 9	43 + 45	Uranus	H214	5.2 × 3.5	60	0.1	Ubach et al. (2012)
	Aug 12	43 + 45	PKS B1934−638	H75	14.6 × 10.3	60	0.1	This work
	Oct 12	43 + 45	PKS B1934−638	H214	5.0 × 3.6	60	0.03	This work
	Oct 12	17 + 19	PKS B1934−638	H214	13.1 × 9.8	90	0.02	This work
MY Lup	Aug 8	44.2 + 46.2	Uranus	H214	4		0.1	Lommen et al. (2010)
	May 9	43 + 45	Uranus	H214	4.8 × 3.4	50	0.1	Ubach et al. (2012)
	Aug 12	43 + 45	PKS B1934−638	H75	14.8 × 10.5	50	0.1	This work
	Oct 12	43 + 45	PKS B1934−638	H214	4.7 × 3.4	80	0.03	This work
	Oct 12	17 + 19	PKS B1934−638	H214	13.6 × 9.7	40	0.02	This work
GQ Lup	2010 Aug 21	43 + 45	Uranus	H168	6.7 × 4.4	80	0.04	Ubach et al. (2012)
	2011 Jul 10	43 + 45	Uranus	H214	6.8 × 3.6	18	0.07	Ubach et al. (2012)
	2012 Aug 4	43 + 45	PKS B1934−638	H75	22.2 × 9.2	53	0.05	This work
	2012 Oct 22	43 + 45	PKS B1934−638	H214	5.0 × 3.6	30	0.04	This work
	2011 July 8	17 + 19	PKS B1934−638	H214	18.3 × 9.7	24	0.01	Ubach (2014)
	2011 July 18	17 + 19	PKS B1934−638	H214	17.8 × 9.1	20	0.02	Ubach (2014)
	2012 Oct 22	17 + 19	PKS B1934−638	H214	13.2 × 9.4	30	0.03	This work

Table A2. ATCA observing log for Chamaeleon sources from this work and the literature. (1) Source name. (2) Date of observation. (3) Frequency pair. (4) Flux calibrator. (5) ATCA array configuration. (6) Synthesized beam size. (7) Total integration time used for analysis. (8) rms. (9) Reference.

Source	Date	Frequency pair (GHz)	Flux Calibrator	Antenna(s) Configuration	Beam size arcsec	T_{int} (min)	rms (mJy beam^{-1})	Reference
CR Cha	May 9	43 + 45	Uranus	H214	5.0 × 4.3	80	0.1	Ubach et al. (2012)
	Aug 12	43 + 45	PKS B1934−638	H75	16.3 × 10.6	20	0.1	This work
CS Cha	2008 Apr 26	43 + 45	PKS B1921−293	6A	2.4 × 1.4	413	0.1	Lommen et al. (2009)
	2008 Jul 5	43 + 45	Uranus	1.5B	11.3 × 0.6	49	0.2	Lommen et al. (2009)
	2008 Jul 6	43 + 45	Uranus	1.5B	4.5 × 0.6	103	0.2	Lommen et al. (2009)
	May 9	43 + 45	Uranus	H214	5.0 × 4.3	80	0.1	Ubach et al. (2012)
	Aug 12	43 + 45	PKS B1934−638	H75	15.9 × 10.3	20	0.1	This work
	Oct 12	43 + 45	PKS B1934−638	H214	5.4 × 4.1	80	0.3	This work
	Jul 11	17 + 19	PKS B1934−638	H214	15.5 × 12.6	105	0.1	Ubach et al. (2012)
	Oct 12	17 + 19	PKS B1934−638	H214	13.9 × 11.4	126	0.03	This work
DI Cha	May 9	43 + 45	Uranus	H214	4.8 × 4.2	100	0.1	Ubach et al. (2012)
	Aug 12	43 + 45	PKS B1934−638	H75	13.8 × 10.7	30	0.1	This work
T Cha	May 9	43 + 45	Uranus	H214	5.1 × 4.1	60	0.1	Ubach et al. (2012)
	Aug 12	43 + 45	PKS B1934−638	H75	17.0 × 10.4	30	0.1	This work
	Jul 11	9	PKS B1934−638	H214	3.2 × 1.1	170	0.1	Ubach et al. (2012)
	Jul 12	9	PKS B1934−638	H168	5.3 × 1.1	20	0.05	This work
	Jul 11	5.5	PKS B1934−638	H214	3.4 × 1.9	170	0.1	Ubach et al. (2012)
	Jul 12	5.5	PKS B1934−638	H168	8.9 × 1.7	20	0.08	This work
Glass I	May 9	43 + 45	Uranus	H214	4.9 × 4.1	150	0.1	Ubach et al. (2012)
	Aug 12	43 + 45	PKS B1934−638	H75	14.0 × 11.4	30	0.1	This work
SZ Cha	May 9	43 + 45	Uranus	H214	5.0 × 4.1	200	0.1	Ubach et al. (2012)
	Aug 12	43 + 45	PKS B1934−638	H75	14.1 × 11.0	40	0.1	This work
	Oct 12	43 + 45	PKS B1934−638	H214	5.4 × 4.0	100	0.1	This work
	Oct 12	17 + 19	PKS B1934−638	H214	13.7 × 11.3	160	0.02	This work
Sz 32	2008 March 31	43 + 45	QSO B1057−797	H168	5.8 × 5.3	119	0.2	Lommen et al. (2010)
	May 9	44 + 45	Uranus	H214	5.0 × 4.0	130	0.2	Ubach et al. (2012)
	Aug 12	43 + 45	PKS B1934−638	H75	14.6 × 11.3	20	0.1	This work
	July 11	9	PKS B1934−638	H214	2.4 × 1.8	125	0.1	Ubach et al. (2012)
	July 12	9	PKS B1934−638	H168	1.5 × 1.0	20	0.05	This work
	July 11	5.5	PKS B1934−638	H214	3.2 × 2.0	125	0.1	Ubach et al. (2012)
	July 12	5.5	PKS B1934−638	H168	3.3 × 1.7	20	0.04	This work
WW Cha	May 9[a]	43 + 45	Uranus	H215	5.0 × 4.0	130	0.2	Ubach et al. (2012)
	Aug 12	43 + 45	PKS B1934−638	H75	17.4 × 10.6	20	0.1	This work
	July 11[a]	9	PKS B1934−638	EW352	2.4 × 1.8	125	0.1	Ubach (2014)
	July 12[a]	9	PKS B1934−638	H168	1.5 × 1.0	20	0.05	This work
	July 11[a]	5.5	PKS B1934−638	EW352	3.2 × 2.0	125	0.1	Ubach (2014)
	July 12[a]	5.5	PKS B1934−638	H168	3.3 × 1.7	20	0.04	This work

Note. [a]WW Cha was not the primary target but was in the field of Sz 32.

APPENDIX B: RESULTS AT 15 MM

Table B1. Summary of single 15 mm band observations. (1) Source name. (2) Date of observation. (3) Total integration time used to determine flux. (4) Combined frequency. (5) Point flux (3σ upper limit for non-detections). (6) rms. (7) Beam size. (8) ATCA array configuration.

(1) Source	(2) Date	(3) T_{int} (min)	(4) Frequency (GHz)	(5) Flux (mJy)	(6) rms (mJy beam^{-1})	(7) Beam size (arcsecs)	(8) Array configuration
SZ Cha	Oct 12	160	18	0.14 ± 0.03	0.02	13.7 × 11.3	H214
Sz 111	Oct 12	90	18	0.08 ± 0.02	0.02	13.1 × 9.8	H214
MY Lup	Oct 12	40	18	<0.06	0.02	13.6 × 9.7	H214

APPENDIX C: SUMMARY OF WW CHA RADIO MONITORING

Table C1. Summary of results for WW Cha monitoring. (1) Source name. (2) Observation date. (3) Total integration time used to determine flux. (4) Frequency. (5) Point flux (3σ for non-detections). (6) rms. (7) Beam size. (8) ATCA array configuration. (9) References.

(1) Source	(2) Date	(3) T_{int} (minutes)	(4) Frequency (GHz)	(5) Flux (mJy)	(6) rms (mJy beam^{-1})	(7) Beam size (arcsecs)	(8) Array Configuration	(9) References
WW Cha	2007 Oct 5	81.0	40.8	3.93 ± 0.29	0.35	11×11	H75C	Lommen, Wright & Maddison (2007)
	2008 Mar 31	119.4	40.8	5.19 ± 0.17	0.194	6.1×5.6	H168	Lommen et al. (2007)
	2007 Oct 5	81.0	42.5	5.41 ± 0.32	0.313	11×11	H75C	Lommen et al. (2007)
	2008 Mar 31	119.4	42.5	5.10 ± 0.17	0.231	5.8×5.3	H168	Lommen et al. (2007)
	May 9	130	44	3.4 ± 0.1	0.2	5.0×4.0	H215	Ubach et al. (2012)
	Aug 12	20.0	44	3.9 ± 0.2	0.1	17.4×10.6	H75	This work
	Jul 11	70.0	18	0.75 ± 0.02	0.1	15.6×12.3	H214	Ubach et al. (2012)
	2006 May 8	48.0	18.4	1.04 ± 0.30	0.158	23×6	H214C	Lommen et al. (2007)
	2006 Oct 13	78.6	18.4	1.08 ± 0.21	0.217	26×9	H214C	Lommen et al. (2007)
	2006 Oct 18	199.2	18.4	1.23 ± 0.19	0.11	39×7	EW352	Lommen et al. (2007)
	2007 Oct 24	189.0	18.4	0.95 ± 0.13	0.181	13×9	H214C	Lommen et al. (2007)
	2007 Nov 2	508.8	18.4	0.48 ± 0.13^{c}	0.089	2.0×1.4	1.5A	Lommen et al. (2007)
	2008 Mar 31	79.8	18.4	1.07 ± 0.10	0.227	15×13	H168	Lommen et al. (2007)
	2006 May 8	48.0	18.5	1.16 ± 0.31	0.329	23×6	H214C	Lommen et al. (2007)
	2006 Oct 13	78.6	18.5	<0.921	0.307	25×9	H214C	Lommen et al. (2007)
	2006 Oct 18	199.2	18.5	0.81 ± 0.20	0.222	38×7	EW352	Lommen et al. (2007)
	2007 Oct 24	189.0	19.4	1.01 ± 0.16	0.209	12×8	H214C	Lommen et al. (2007)
	2007 Nov 2	508.8	19.4	0.55 ± 0.20^{c}	0.125	1.9×1.3	1.5A	Lommen et al. (2007)
	2008 Mar 31	79.8	19.4	0.88 ± 0.12	0.232	14×13	H168	Lommen et al. (2007)
	Jul 11	125.0	9.9	<0.3	0.1	2.4×1.8	EW352	Ubach et al. (2012)
	Jul 12	20.0	9.9	<0.15	0.05	1.5×1.0	H168	This work
	2006 Oct 18	237.0	8.6	<0.222	0.074	71×20	EW352	Lommen et al. (2007)
	2007 June 9	311.4	8.6	0.63 ± 0.06	0.076	53×16	EW352	Lommen et al. (2007)
	Jul 11	125.0	5.5	<0.24	0.1	3.2×2.0	EW352	Ubach et al. (2012)
	Jul 12	20.0	5.5	<0.12	0.04	3.3×1.7	H168	This work
	2006 Oct 18	237.0	4.8	<0.202	0.067	125×32	EW352	Lommen et al. (2007)
	2007 June 9	311.4	4.8	<0.399	0.133	91×26	EW352	Lommen et al. (2007)

This paper has been typeset from a TEX/LATEX file prepared by the author.